Electrochemical properties and optical transmission of high Li+ conducting LiSiPON electrolyte films

Su, Y.; Falgenhauer, J.; Leichtweiß, T.; Geiß, M.; Lupó, C.; Polity, A.; Zhou, S.; Obel, J.; Schlettwein, D.; Janek, J.; Meyer, B.;

Originally published:

September 2016

Physica Status Solidi (B) 254(2017)2, 1600088

DOI: https://doi.org/10.1002/pssb.201600088

Electrochemical properties and optical transmission of high Li^+ conducting LiSiPON electrolyte films

Yurong Su[*,1], Jane Falgenhauer[2], Thomas Leichtweiß[3], Matthias Geiß[3], Christian Lupó[2], Angelika Polity[,1], Shengqiang Zhou[4], Jaroslava Obel[5], Derck Schlettwein[2], Jürgen Janek[3] and Bruno K. Meyer[T,1]**

[1] 1st Physics Institute, Justus-Liebig-University, Heinrich-Buff-Ring 16, 35392 Giessen, Germany
[2] Institute of Applied Physics, Justus-Liebig-University, Heinrich-Buff-Ring 16, 35392 Giessen, Germany
[3] Institute of Physical Chemistry, Justus-Liebig-University, Heinrich-Buff-Ring 58, 35392 Giessen, Germany
[4] Helmholtz-Zentrum Dresden-Rossendorf, Institute of Ion Beam Physics and Materials Research, Bautzner Landstr. 400, 01328 Dresden, Germany
[5] Department of Chemistry, University of Munich (LMU), Butenandtstr. 5-13, 81377 München, Germany

Received ZZZ, revised ZZZ, accepted ZZZ
Published online ZZZ (Dates will be provided by the publisher.)

Keywords: LiSiPON; inorganic solid electrolyte; lithium microbattery; electrochemical properties.

* Corresponding author: e-mail Yurong.Su@exp1.physik.uni-giessen.de, Phone: +49(0)641 99 33116, Fax: +49(0)641 99 33139
** e-mail Angelika.Polity@exp1.physik.uni-giessen.de, Phone: +49(0)641 99 33117, Fax: +49(0)641 99 33139
[T]Deceased.

Lithium silicon phosphorus oxynitride (LiSiPON) thin films with different compositions have been prepared by RF magnetron sputtering in N_2 by using three targets $xLi_2SiO_3 \cdot (1-x)Li_3PO_4$ with x=0.1, 0.3 and 0.5. Compared with LiPON, the electrical properties of LiSiPON have been improved by introducing silicon. LiSiPON films deposited from the target $0.5Li_2SiO_3 \cdot 0.5Li_3PO_4$ yield the highest ionic conductivity of up to 9.7×10^{-6} S/cm with an activation energy of only 0.41 eV. The main mechanism for increasing ionic conductivity is the enhancement of carrier mobility. By DC polarization measurements the electronic partial conductivity was found at least 7 orders of magnitude smaller than the ionic conductivity. Linear voltammetry results showed that the LiSiPON films are electrochemically stable in contact with stainless steel in the voltage range of 0-6 V. The substitution of silicon for phosphorus in the film evidenced from X-ray photoelectron spectroscopy analysis indicated silicon in the film will create more abundant cross-linking structures Si-O-P and (P,Si)-N<(P,Si), hence created more Li^+ conducting paths which favored the higher mobility of lithium ions and larger ionic conductivity. The optical bandgap was found to decrease with increasing silicon content. We demonstrate that the prepared LiSiPON films with their larger ionic conductivity and low electronic conductivity may serve as an alternative to LiPON for applications in high energy density and high voltage lithium batteries.

1 Introduction Lithium microbatteries are all-solid-state thin film devices, which are undergoing an increasing market demand as power sources for miniaturized systems. A typical lithium microbattery is composed of a high voltage cathode, a glassy or ceramic Li^+ conductor thin film as the electrolyte, and an anode which may be Li metal or an intercalation compound. Tremendous research has been undertaken on investigations of inorganic electrolytes for microbatteries[1]. Among various lithium electrolyte materials, glassy lithium phosphorous oxynitride (LiPON) is one of the best choices for lithium microbatteries[2,3]. By vapor deposition of the component elements, the film composition can be tuned and the ionic conductivity can reach 10^{-5} S/cm[4]. However, the ionic conductivity of LiPON films prepared by other techniques, for instance sputtering, falls in the range between 10^{-7} and 10^{-6} S/cm at room temperature[1,5], due to during the sputtering process it is difficult to control the exact composition of thin films. However, careful adjustment of the preparation conditions can lead to increased conductivity. Recently we prepared LiPON films by RF magnetron sput-

tering from a Li_3PO_4 target in N_2 with an ionic conductivity of 4.9×10^{-6} S/cm at room temperature[6].

Compared with the Li-P-O system, the increased ionic conductivity in LiPON was attributed to the substitution of oxygen atoms of the PO_4 groups with nitrogen in the glassy network[3,7]. Besides, the substitution of Si^{4+} for P^{5+} could further enhance the mobility of Li ions[2]. Lee *et al.*[8] reported that by introducing silicon into LiPON, the ionic conductivity of such LiSiPON films can reach 10^{-5} S/cm. Moreover a thin film battery device with the structure of $LiCoO_2$/LiSiPON/SiV was successfully demonstrated [9]. However, details of the physical and chemical properties of LiSiPON, for instance the electronic conductivity, the relationship between the microstructure and the properties of LiSiPON have not been well established and understood.

Aside from their use in lithium batteries, lithium phosphate based inorganic electrolytes are also suitable for use in solid-state electrochromic (EC) devices[10] because of a high optical transmission in the UV-Vis range[3]. Therefore, the optical transmission of the electrolyte is also relevant to investigate.

In the present paper, LiSiPON films have been successfully prepared by RF sputtering from targets with different Si/P ratio of 1/9, 3/7 and 1/1. The film composition, the electrochemical properties and optical transmission of LiSiPON films were evaluated in detail. The correlations between composition, local structure and film performances were established.

2 Experimental Sputtering targets were prepared by cold pressing well-mixed powders of Li_2SiO_3 and Li_3PO_4 (Sigma-Aldrich) in the appropriate ratio and subsequent sintering of the tablets at 1050 ˚C in air. The targets with different parts of fractions of Li_2SiO_3 and Li_3PO_4 powder can be represented by $xLi_2SiO_3\cdot(1-x)Li_3PO_4$, with x= 0.1, 0.3, and 0.5. Hereafter, the three corresponding targets are referred to as 0.1-LiSiPO, 0.3-LiSiPO and 0.5-LiSiPO, respectively.

As substrate 1×1 cm^2 silica glass and float glass were mounted at 5.3 cm distance of the sputter target. The base pressure of the process chamber was 10^{-7} mbar. LiSiPON films were deposited by reactive RF magnetron sputtering in N_2 (99.99%) atmosphere neither intentionally heating nor cooling of the substrate. The N_2 pressure and RF power were varied in order to optimize the ionic conductivity. As deposition conditions for the films with the highest ionic conductivity for all three targets was found to be an RF power of 50 W at a N_2 pressure of 1×10^{-3} mbar. Under these sputter conditions, the growth rate of the film was determined to be about 6 nm/min. The corresponding samples with the highest ionic conductivity prepared from 0.1-LiSiPO, 0.3-LiSiPO and 0.5-LiSiPO targets are referred to as type A, type B and type C, respectively. Three specimens of each type were prepared and they differed in their conductivity by not more than 10%. In the following, a representative sample is shown when a given type of samples is referred.

The surface morphology and cross sectional views of LiSiPON films were observed by scanning electron microscopy (SEM) by use of a Jeol JSM 7001F thermal field SEM from *Zeiss*. Si/P, O/P and N/P ratios were determined by Rutherford backscattering spectrometry (RBS, Helmholtz-Zentrum Dresden-Rossendorf). The Li/P ratio was determined by inductively coupled plasma-optical emission spectrometry (ICP-OES) method using a Varian Vista RL CCD simultaneous ICP-AE-spectrometer (now *Agilent*) with radial Ar plasma, patented Vista Chip-CCD detector features and Echele optics. The optics is thermostated and surrounded with N_2 gas for less noise in spectra. For determination of the ionic and electronic conductivities, 100 nm thick stainless steel (SS) electrodes were deposited by RF sputtering from a SS target in Ar (99.99%). SS/LiSiPON/SS sandwich structures were prepared on glass substrates with an active area of 4 mm^2. The thickness of LiSiPON films for all of the electrochemical measurements was around 1.1 µm as concluded from cross-section SEM and optical transmission. Electrochemical impedance spectroscopy (EIS) was performed from room temperature to 65 ˚C with an increment of 5 ˚C using a *Zahner* IM6 electrochemical workstation. The electronic partial conductivity was measured by DC polarization technique. By applying a constant voltage drop to the sample for 48 hours, the current response was recorded over time using a *Keithley* 6430 source meter. In order to minimize environmental influences the samples were placed in a faraday cage, which was positioned inside a climatic chamber (*Binder*) to ensure a constant temperature of 25 °C.

The chemical structure of the films was probed using X-ray photoelectron spectroscopy (XPS) carried out with a PHI 5000 Versaprobe Scanning ESCA Microprobe (*Physical Electronics*) at a chamber pressure in the range of 10^{-8} mbar using monochromatic Al K_α radiation. The analyzer was operated at a constant pass energy of 23.50 eV for detailed and at 187.85 eV for survey spectra, respectively. The UV-Vis optical transmittance was measured for LiSiPON films deposited on silica substrates using a *Perkin-Elmer* Lambda 900 spectrometer with air as reference.

3 Results and discussions

3.1 Morphology and compositions Films prepared at optimized conditions showed a very homogeneous texture (Fig. 1). They were uniform and compact, without any cracks or pin holes which is beneficial for an optimized transport of lithium ions.

The compositions of LiSiPON in the different films types prepared under optimized conditions from each target are summarized in Table 1. Very systematic trends in the chemical composition of the films were established. We found that the Si content in the films increased monotonically as the portion of Li_2SiO_3 in the targets increased, and the Si/P ratio in the films was close to the nominal target composition which means equal sputter rates for Si and P were established.

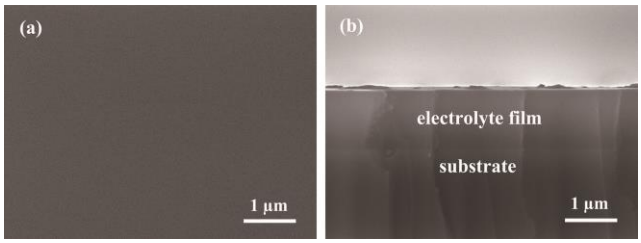

Figure 1 Surface and cross-sectional SEM images of a type C sample.

Table 1 Atomic concentration of LiSiPON films deposited from three targets measured by ICP-OES. The concentration of our LiPON film[6] was also listed for comparison.

Target	Type	Atomic concentrations (at. %)					Si/P
		Li	Si	P	O	N	
Li_3PO_4	LiPON[6]	43.4	-	13.9	23.4	19.3	-
0.1-LiSiPO	A	47.6	1.0	12.2	20.6	18.6	0.08
0.3-LiSiPO	B	41.6	3.9	9.9	27.2	17.4	0.40
0.5-LiSiPO	C	46.1	6.9	7.4	23.8	15.8	0.93

3.2 Electrochemical properties Temperature dependent impedance spectroscopy was applied to study the ionic conductivity of LiSiPON. A representative Nyquist plot of the electrolyte film between a pair of SS electrodes is shown in the inset of Fig. 2. Values of the bulk conductivity were fitted from EIS data by using an established equivalent circuit[6]. The activation energy E_a is estimated based on the Arrhenius equation for the ionic conductivity: $\sigma_{dc}T = F_0\exp(-E_a/k_BT)$, where σ_{dc} is the ionic conductivity(or DC conductivity), F_0 is a pre-exponential factor, T is the absolute temperature and k_B is the Boltzmann constant. F_0 and E_a are directly related to the concentration of mobile ions and the mobility respectively. Arrhenius plots of $\log(\sigma T)$ as a function of $1000/T$ and the corresponding fits are shown in Fig. 2 for sample types A, B and C. The ionic conductivities at room temperature, the pre-exponential factor F_0 and E_a are listed in Table 2. The result of our previous study on LiPON[6] is also listed for comparison purposes.

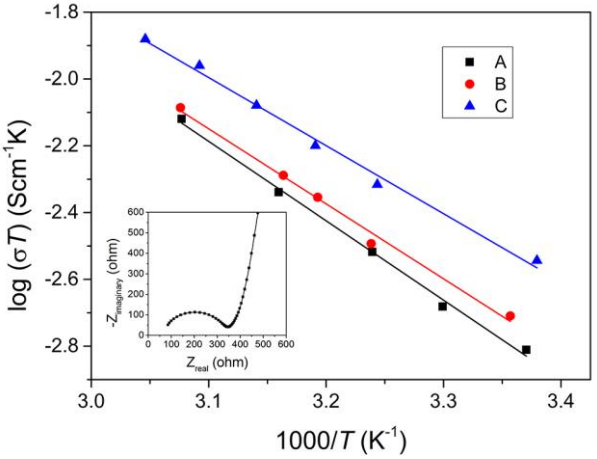

Figure 2 Arrhenius plots of $\sigma_{dc}T$ of LiSiPON samples. The inset shows a typical impedance spectrum of a SS/LiSiPON/SS cell.

Table 2 Room temperature ionic conductivity σ_{dc}, pre-exponential factor F_0, and activation energy E_a of LiSiPON electrolyte films. The corresponding value for the LiPON film is also listed as reference.

Type	σ_{dc} (S/cm) at 25 °C	F_0 (K S/cm)	E_a (eV)	Si/P
LiPON[6]	4.9×10^{-6}	3.3×10^{6}	0.55	-
A	5.4×10^{-6}	1.5×10^{5}	0.47	0.08
B	6.6×10^{-6}	7.9×10^{4}	0.45	0.40
C	9.7×10^{-6}	2.5×10^{4}	0.41	0.93

From Table 2, the introduction of Si into LiSiPON led to significant improvement ionic conductivity compared with LiPON, and the conductivity is further increased with increasing Si content. At a Si/P ratio of 0.93, the room temperature conductivity can reach 9.7×10^{-6} S/cm, and the corresponding E_a is around 0.41 eV. It is clear that the mixture of former materials in the target and, hence, in the thin films indeed can improve the electrochemical properties substantially. The pre-exponential factor F_0 decreases with increasing Si content and this would have negative effects on the ionic conductivity. Thus the observed increase of ionic conductivity should be attributed to higher lithium ion mobility. Similar to previous nitrogen or silicon doped lithium phosphate[2,11,12], the evolution of ionic conductivity and activation energy have also been attributed to an improvement of the lithium ion mobility rather than the increase of mobile lithium ions in the thin films. These results are also in agreement with the theoretical calculations on lithium phosphate compounds[13,14], in

which the authors claimed the migration energy of lithium ions can be lowered down due to a structural change induced by substituting N and Si for O and P in Li_3PO_4. Detailed XPS analyses allowed us to focus on such chemical structural change of LiSiPON films described afterwards.

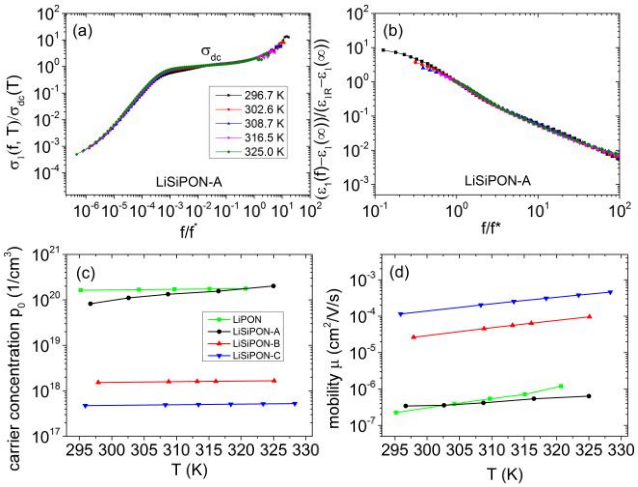

Figure 3 (a) Conductivity and (b) permittivity master curves for LiSPON-A. (c) Temperature dependence of carrier concentration p_0 and (d) Temperature dependence of carrier mobility μ for LiPON (Green) and LiSiPON-A (Black), B (Red), and C (Blue).

Furthermore, in order to obtain more detailed information of temperature dependence of ionic conductivity mechanism, we analyze the complex impedance by following the method described in reference[15,16]. The carrier concentration p_0 and the mobility μ can be calculated from the conductivity and permittivity as a function of frequency. Conductivity and permittivity are calculated from the impedance data by the following equations:

$$\sigma(f) = \sigma_1(f) + i\sigma_2(f) = \frac{d}{A}\frac{1}{Z};$$

$$\varepsilon(f) = \varepsilon_1(f) - i\varepsilon_2(f) = \frac{\sigma(f)}{i2\pi f \varepsilon_0}$$

where f is the frequency, Z is the measured complex impedance, d and A are the thickness and area of film, ε_0 is the vacuum permittivity.

As a demonstration, the master curves of conductivity and permittivity for LiSiPON-A are shown in Fig. 3 (a) and (b). After being rescaled the conductivity and permittivity at different temperature follow approximately into a single curve. This is a typical feature of ionic conducting behavior in amorphous electrolyte[16]. For example, in the low-frequency the conductivity has a feature of electrode polarization, while in the middle frequency the conductivity show a flat platform corresponding to the ionic conductivity. The carrier concentration p_0 can be evaluated from the permittivity master curves as shown in Fig. 3(c). For LiPON and LiSiPON-A the mobile carrier concentration is at the order of 10^{20} cm^{-3}. This value is similar to the typical value in LiPON film[15]. However for LiSiPON-B and LiSiPON-C, which have higher Si content in the films, the carrier concentration density decreased to the order of 10^{18} cm^{-3}. At the other hand, as it is shown in Fig. 3(d) the carrier mobility μ of LiPON and LiSiPON-A is in the range of 10^{-7}-10^{-6} $cm^2V^{-1}s^{-1}$, while for LiSiPON-B and LiSiPON-C it is increased to the range of 10^{-5}-10^{-4} $cm^2V^{-1}s^{-1}$.

The main conclusions from the analysis of temperature dependence of impedance implies that: (1) The ionic conducting mechanism in LiSiPON films are the same as in LiPON or other inorganic electrolytes. (2) The leading factor on the improvement of ionic conductivity in LiSiPON film is the increase of the mobility with increasing of Si content. This conclusion is consistent with the prefactor and activation energy analysis discussed previously.

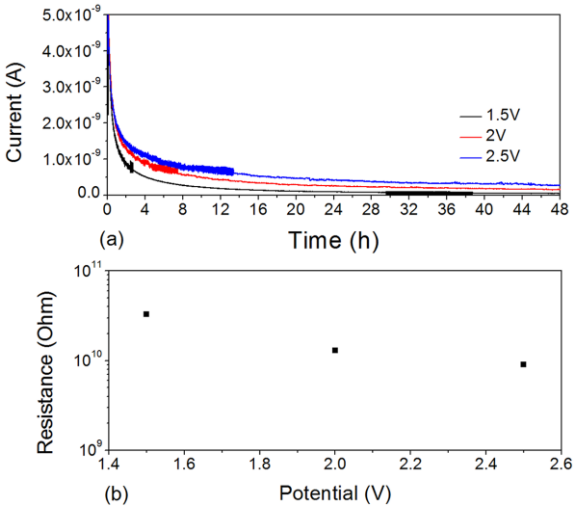

Figure 4 Current transient curves (a) for a sample of type C at a polarization potential of 1.5 V, 2 V and 2.5 V and the calculated dc resistance (b) as a function of the applied potential at room temperature (25 °C).

A solid electrolyte with high ionic conductivity and, however, negligible electronic contribution is required in batteries as well as EC devices to avoid internal short circuit and self-discharge. Thus, it is crucial to determine the electronic transfer number in a given material. DC potentials of 1.5 V, 2 V, and 2.5 V were applied to samples of type C, and the current-time decay curves were recorded for 48 hours until a steady-state current was reached as shown in Fig. 4a. At this state, the current arises from electronic leakage only, since two ion-blocking SS electrodes were used. Fig. 4b shows the obtained DC resistance values as a function of the applied voltage. An electronic conductivity (σ_e) of 2.6×10^{-13}

S/cm was determined. Thus, LiSiPON can be considered as a pure ion conductor. It should be mentioned that these polarization measurements between two ion-blocking electrodes do not resemble a real Wagner-Hebb measurement but instead provide an upper limit of the electronic partial conductivity.

In addition, the electrochemical stability window was evaluated from linear sweep voltammetry. Fig. 5 shows an current-voltage (*I-V*) scan curve of a LiSiPON sample of type C, which was measured at room temperature with a scan rate of 1 mV/s. The current increased dramatically when the potential exceeds 6.0 V. The onset of the current flow beyond 6.0 V may be associated with the decomposition of LiSiPON. We assume a stability window of LiSiPON is 6.0 V which suggest it is suitable for high voltage lithium battery application.

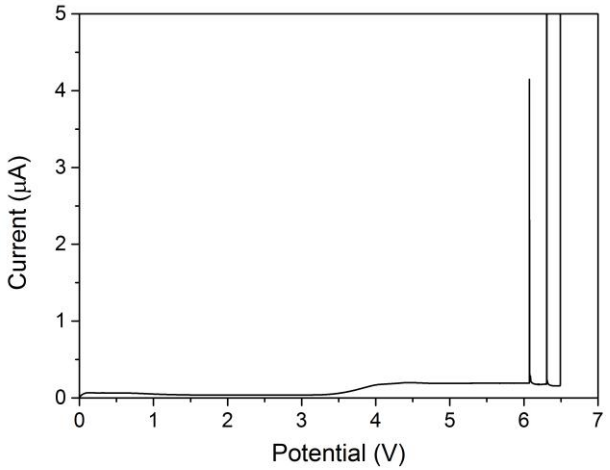

Figure 5 Linear sweep voltammogram of a type C sample between a pair of SS electrodes with a scan rate of 1 mV/s.

3.3 XPS survey of Chemical structure XPS was carried out in order to further investigate the chemical composition and reveal the details of chemical bonds. All elements (Li, P, Si, O and N) in LiSiPON film were successfully detected as seen in the survey spectra of a sample of type C in Fig. 6. Representative analysis of XPS spectra of the O1s, N1s, P2p and Si2p peak regions are given in Fig. 7 in order to demonstrate the impact of Si dose on the binding environment of the sputtering films.

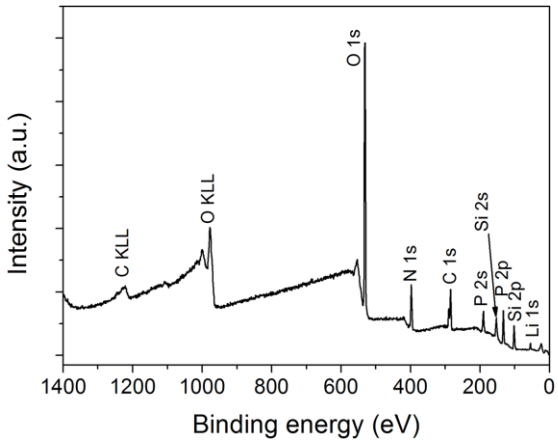

Figure 6 XPS survey spectrum of a type C sample.

The P2p spectra from LiSiPON are consistent with LiPON. It has two peaks representing the $2p_{1/2}$ and $2p_{3/2}$ (0.8 eV lower than $2p_{1/2}$[17]) contributions to the phosphorus bonding in PN_xO_{4-x} tetrahedron. Studies on XPS of LiPON showed a reduction in P2p binding energy of Li_3PO_4 when P-O bonds are gradually replaced by P-N bonds, which change the charge distribution around phosphorus in thin films[18,19]. In Fig. 7 and Table 3, the $P2p_{3/2}$ XPS peak of LiPON shifted up in energy from 132.4 to 132.9 eV upon the Si/P ratio reach to 0.93. This is probably due to the loss of P-N bonds.

Three main peaks can be seen in the Si2p spectral region. The first peak positioned at 101.7 eV can be assigned to the Si-N_4 (S1) tetrahedron (Si_3N_4). The second peak located between 101.7-103.0 eV is associated to the O_x-Si-N_y (S2) tetrahedron. This peak position shifted up from 102.3 to 102.6 eV when the Si/P atomic ratio is increased from 0.08 to 0.93. This indicates a substitution of a nitrogen atom by an oxygen atom in the O_x-Si-N_y tetrahedron[20,21]. In addition, the third peak observed at 100.8 eV is related to the Si-O-Li (S3) bond in Li silicates (possibly Li_4SiO_4)[23,24]. In order to obtain quantitative information of each bonding states, we can define the area under the Gaussian-Lorentzian curve in the XPS as a quantitative measurement of the amount of each bonding state. As it is shown in Table 3, with increasing Si/P ratio, the contribution of the Si-N_4 species does not show obvious change for the three LiSiPON films, while the decrease of the Si-O-Li is counter-balanced by the increase of the O_x-Si-N_y tetrahedron species. We did not find obvious peak related to SiO_2 (Si-O_4 tetrahedron), which should be positioned at above 103.0 eV[20-22].

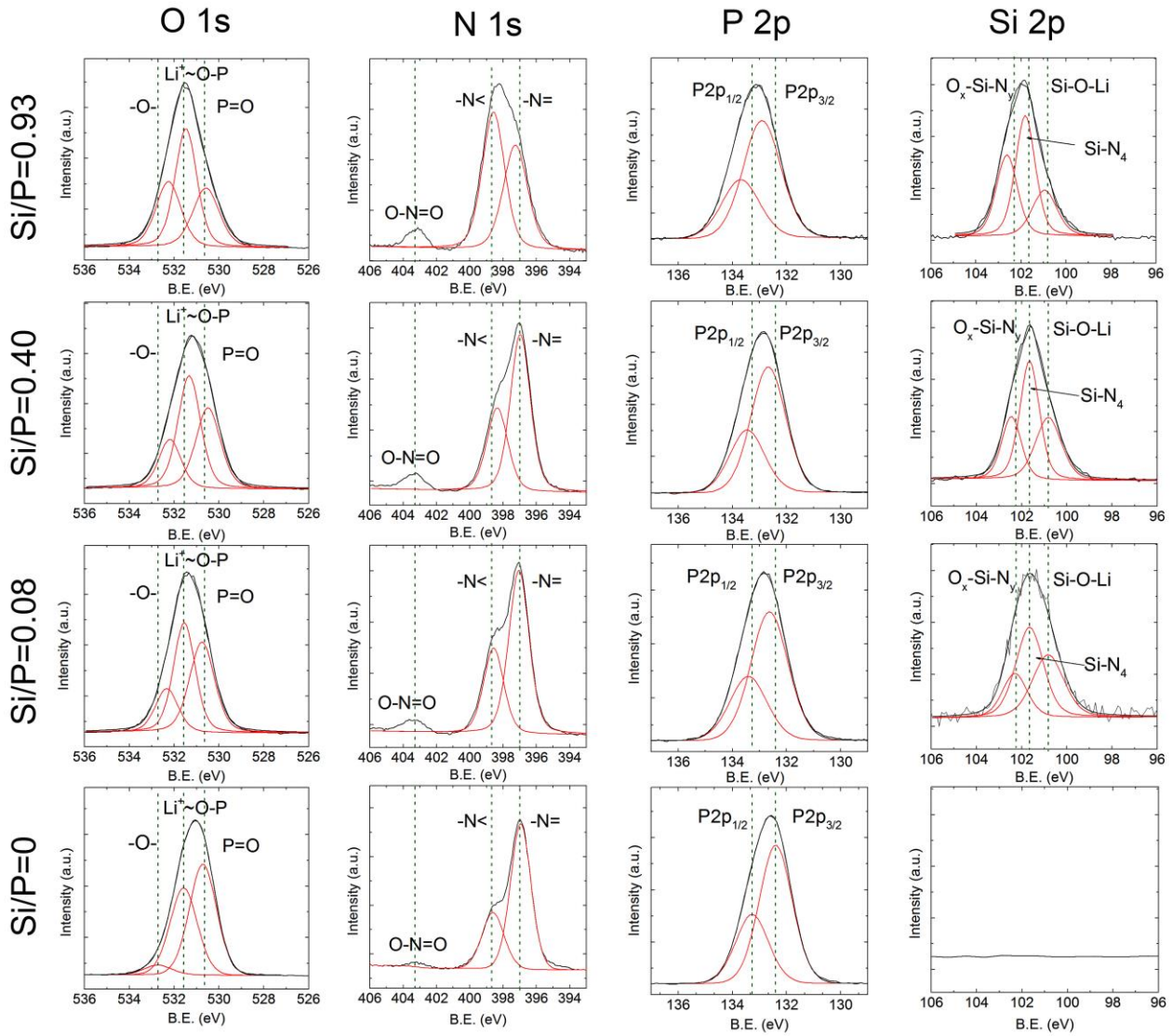

Figure 7 High-resolution core-level XPS spectra (columns) of LiSiPON and LiPON films. Each spectrum is comprised of multiple peaks.

Table 3 Phosphorus, silicon, oxygen and nitrogen bonding characteristics of LiSiPON samples in this work and LiPON from Ref. [6].

Sample type	P	Si		O		N	
	B.E. (eV)	B.E. (eV)	%	B.E. (eV)	%	B.E. (eV)	%
LiSiPON A	$P2p_{1/2}$ 133.4	S1 101.7	44.7	BO 532.3	17.6	Nd 397.0	62.9
	$P2p_{3/2}$ 132.6	S2 102.3	19.9	NBO1 530.7	40.2	Nt 398.6	32.8
		S3 100.8	35.4	NBO2 531.6	42.2	N_o 403.5	4.3
LiSiPON B	$P2p_{1/2}$ 133.5	S1 101.7	45.0	BO 532.2	19.3	Nd 397.0	57.6
	$P2p_{3/2}$ 132.7	S2 102.5	23.4	NBO1 530.5	35.5	Nt 398.4	36.7
		S3 100.8	31.6	NBO2 531.4	45.2	N_o 403.4	5.7
LiSiPON C	$P2p_{1/2}$ 133.7	S1 101.8	45.5	BO 532.3	28.1	Nd 397.2	43.2
	$P2p_{3/2}$ 132.9	S2 102.6	32.6	NBO1 530.6	27.4	Nt 398.6	52.0
		S3 100.9	21.9	NBO2 531.5	44.5	N_o 403.3	4.8
LiPON[6]	$P2p_{1/2}$ 133.3			BO 532.7	4.6	Nd 397.0	70.7
	$P2p_{3/2}$ 132.4			NBO1 530.7	53.4	Nt 398.7	27.9
				NBO2 531.6	42.0	N_o 403.3	1.4

The O1s spectrum of LiPON in Fig. 7 clearly show three components upon decomposition: non-bridging oxygen P=O (NBO1) at 530.7 eV, non-bridging oxygen $Li^+...^-O$-P (NBO2) at 531.6 eV, and bridging oxygen P-O-P (BO) at 532.7 eV. Those peak identifications are consistent with prior XPS results on LiPON films [11,25]. The two NBOs were also observed in our Li-SiPON film, while BO binding energy was shifted down to 532.3 eV. This BO peak can be assigned to Si-O-P[26], indicating silicon ions successfully replace the four-coordinated phosphorus. From Table 3, with an increase of Si/P ratio, the relative proportion of the NBO2 ($Li^+...^-O$-P) does not vary too much whereas NBO1 component (P=O) decreases with BO (Si-O-P) component increase. The formation of heteroatom (Si-O-P) groups increases the network cross-linking[2] which facilitate Li^+ transfer between phosphate chains leading to higher mobility and ionic conductivity.

The N1s spectrum was comprised of three Gaussian-Lorentzian contributions: nitrogen bonded to oxygen (No: O-N=O) at 403.3 eV, triple-coordinated nitrogen –N< (Nt) bonded to P or Si at 398.6 eV, and double-coordinated nitrogen –N= (Nd) bonded to P or Si at 397.0 eV. The relative data of the components are presented in Table 3. In LiPON, the Nd component is predominant. When the silicon content increases, the Nt component increases and becomes predominant, reaching 52% for Si/P equals to 0.93 (LiSiPON type C). It was reported that the replacement of P-N bond in the oxynitride glass makes the ionic conductivity improved by decreasing the electrostatic energy of P-O bond[27]. Compared with Nd structural unit, the formation of Nt unit will remove more P-O bonds[28]. Consequently, the contribution to the decrease of electrostatic energy by Nt structural unit is larger than that by Nd structural unit. Hence the Nt cross-linking structural unit is more responsible than Nd structural unit for the increase in Li^+ mobility.

The main conclusions of above XPS analysis indicate that most of incorporated silicon ions replace the phosphorus ions as four-coordinated tetrahedral units and the nitridation was successfully completed in our Si-P composition range. The combined approach of the mixed silicate and phosphate former effect and nitrogen incorporation is believed to be responsible for improving the electrochemical properties of a LiSiPON glassy film electrolyte.

3.4 Optical transmission In addition to the electrochemical properties, the optical transmission in the UV-Vis range is crucial for the electrolyte in EC devices. A high optical transparency (bandgap energy > 3 eV) is required in the transmission type EC devices[10].

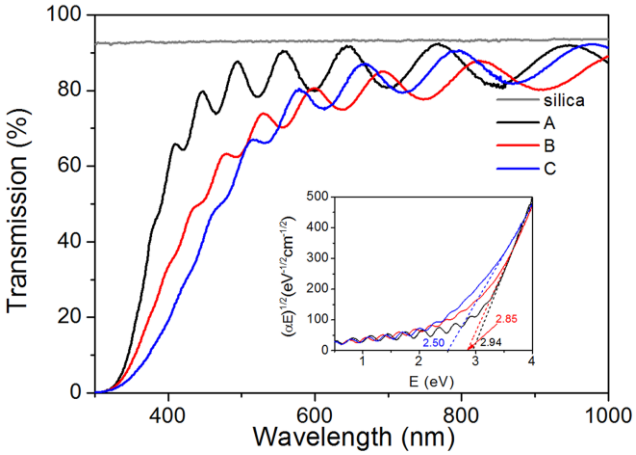

Figure 8 UV-Vis transmission spectra of LiSiPON films on silica glass substrates. The transmission of silica glass substrate is shown as a gray line. The inset shows the Tauc plots and the linear extrapolation to determine the bandgap.

Fig. 8 shows the UV-Vis transmission spectra of LiSiPON films grown on silica glass substrates compared to transmission of the bare silica glass substrate. The interference pattern observed at a higher wavelength range confirms the almost perfectly smooth morphology of the films (Fig. 1). For samples of type A with a small content of silicon, a high transparency above 500 nm and a strong absorption below 400 nm was observed. As the ratio of Si/P increases, a decrease in the transmission can be observed. The large absorption is due to the bandgap absorption. The bandgap energies of samples of type A, B and C are derived to be 2.94, 2.85 and 2.50 eV, respectively, from the Tauc plots shown as inset of Fig. 8. Generally bandgap of the Li-SiPON system follow a decreasing trend with increase in content of Si. In our amorphous LiSiPON film, there are many factors will impact the optical bandgap, for instance composition change of Si, P, O, N, chemical envirement change of Si, P, O, N, and other effects like defects, charge impurities, structure disorder, etc. It is not easy to give a definite explanation for the decrease of bandgap when more Si is incorporated into the film since some factors change at the same time. However we can give a possible hint for the reduction of bandgap based on the change of chemical environment of Si. The bandgap of amorphous film increase from Si-SiO_x-SiO_2[29,30] because of the Si-O bonding. On the other hand, the bandgap decreases from SiO_2-SiO_xN_y-Si_3N_4[31]. This implies that the Si-N bonds leads to decrease of the bandgap. From our Si2p XPS analysis, the Si-N_4 and O_x-Si-N_y ratio increase and the Si-O bond decreases when Si concentration is increase. This may probably explain the decreasing trend of bandgap when

more Si is present in the film. By considering the optical transmission, the LiSiPON electrolyte with low Si concentration (< 10%) which has both high ionic conductivity and high transparency in the UV-Vis range is more suitable as a candidate to be used in transmission type EC devices.

4 Conclusions LiSiPON films with different composition have been successfully prepared by RF sputtering from targets based on different Si/P content. It was shown that silicon doping plays a decisive positive role in increasing the ionic conductivity of this type of solid electrolytes. The best ionic conductivity at room temperature of 9.7×10^{-6} S/cm was achieved with the lowest activation energy of 0.41 eV. The electronic conductivity was negligible and orders of magnitude lower than the ionic conductivity. The prepared LiSiPON films are electrochemically stable up to 6V against stainless steel. The optical bandgap of LiSiPON was found to be reduced relative to LiPON caused by the increased content of silicon in the film. From the XPS analysis more amount of cross-linked structures Si-O-P and (P, Si)-N<(P, Si) were created in mixed phosphate and silicate network, supplying more conducting Li^+ paths with a lower activation energy and higher mobility. The highly advantageous electrical properties clearly suggest that LiSiPON represents a competitive alternative to LiPON in lithium thin film batteries.

Acknowledgments We acknowledge financial support within the LOEWE program of excellence of the Federal State of Hessen (project initiative STORE-E) and the German Federal Ministry of Education and Research (BMBF) within the funding program Photonics Research Germany (contract number 13N13239).

References

[1]. P. Knauth, Solid State Ionics **180**, 911 (2009).
[2]. J. B. Bates, N. J. Dudney, G. R. Gruzalski, R. A. Zuhr, A. Choudhury, C. F. Luck, and J. D. Robertson, Solid State Ionics, **53-56**, 647 (1992).
[3]. X. Yu, J. B. Bates, G. E. Jellison, and F. X. Hart, J. Electrochem. Soc. **144**, 524 (1997).
[4]. Ilika Techonoligies LTD. and Toyota Motor Corporation, WO 2013/011326 A1 (2013).
[5]. J. Li, C. Ma, M. Chi, C. Liang, and N. J. Dudney, Adv. Energy Mater., **5**, 1401408 (2015).
[6]. Y. Su, J. Falgenhauer, A. Polity, T. Leichtweiß, A. Kronenberger, J. Obel, S. Zhou, D. Schlettwein, J. Janek, and B. K. Meyer, Solid State Ionics, **282**, 63-69 (2015).
[7]. J. B. Bates, N. J. dudney, G. R. Gruzaiski, R. A. Zuhr, A. Choudhury, C. F. Luck, and J. D. Robertson, J. Power Sources, **43**, 103 (1993).
[8]. S.-J. Lee, J.-H. Bae, H.-W. Lee, H.-K. Baik and S.-M. Lee, J. Power Sources, **123**, 61-64 (2003).
[9]. H.-K. B. S.-J. Lee, and S.-M. Lee, Electrochem. Commun., **5**, 32-35 (2003).
[10]. C. G. Granqvist, Thin Solid Films **564**, 1 (2014).
[11]. B. Fleutot, B. Pecquenard, H. Martinez, M. Letellier and A. Levasseur, Solid State Ionics, **186**, 29-36 (2011).
[12]. Y-W. Hu, I. D. Raistrick and R. A. Huggins, J. Electrochem. Soc., **124**, 1240-1242 (1977).
[13]. Y. A. Du and N. A. W. Holzwarth, Phys. Rev. B, **78**, 174301 (2008).
[14]. H. Rabaâ, R. Hoffmann, N. C. Hernández and J. F. Sanz, J. Solid State Chem., **161**, 73-79 (2001).
[15]. L.L.Van-Jodin, F.Ducroquet, F.Sabary, I. Chevalier, Solid State Ionics, **253**, 151-156 (2013).
[16]. J.C. Dyre, P. Maass, B. Roling, D.L. Sidebottom, Rep. Prog. Phys. **72**, 1-15 (2009).
[17]. P. D. Mani, S. Saraf, V. Singh, M. Real-Robert, A. Vijayakumar, S. J. Duranceau, S. Seal and K. R. Coffey, Solid State Ionics, **287**, 48-59 (2016).
[18]. Y. G. Kim and H.N.G. Wadley, J. Power Sources, **196**, 1371-1377 (2011).
[19]. C. S. Nimisha, K. Y. Rao, G. Venkatesh, G. M. Rao and N. Munichandraiah, Thin Solid Films, **519**, 3401-3406 (2011).
[20]. J. Dupuis, E. Fourmond, D. Ballutaud, N. Bererd and M. Lemiti, Thin Solid Films, **519**, 1325-1333 (2010).
[21]. P. Cova, S. Poulin, O. Grenier and R. A. Masut, J. Appl. Phys., **97**, 073518 (2005).
[22]. J. Binner and Y. Zhang, J. Mater. Sci. Lett., **20**, 123-126 (2001).
[23]. H. Takezawa, K. Iwamoto, S. Ito and H. Yoshizawa, J. Power Sources, **244**, 149-157 (2013).
[24]. B. Philippe, R. Dedryvère, J. Allouche, F. Lindgren, M. Gorgoi, H. Rensmo, D. Gonbeau and K. Edström, Chem. Mater., **24**, 1107-1115 (2012).
[25]. N. Mascaraque, J. L. G. Fierro, Alicia Durán and Francisco Muñoz, Solid State Ionics, **233**, 73-79 (2013).
[26]. R. M. Almeida, H. C. Vasconcelos, M. C. Gonçalves and L. F. Santos, Journal of Non-Crystalline Solids, **232-234**, 65-71 (1998).
[27]. H. Unuma, K. Komori and S. Sakka, J. Non-Cryst. Solids, **95-96**, 913-920 (1987).
[28]. B. C. Bunker, D. R. Tallant, C. A. Balfe, R. J. Kirkpatrick, G. L. Turner and M. R. Reidmeyer, J. Am. Ceram. Soc., **70**, 675-681 (1987).
[29]. A. Barranco, F. Yubero, J. P. Espinos, P. Groening and A. R. Gonzalez-Elipe, J. Appl. Phys. **97**,113714 (2005).
[30]. H. R. Philipp, J. Phys. Chem. Solids, **32**, 1935-1945 (1971).
[31]. A. N. Sorokin, A. A. Karpushin, V. A. Gritsenko, and H. Wong, J. Appl. Phys. **105**, 073706 (2009).